

等离子喷涂法制备铁基硬质涂层的力学性能

雷阿利, 冯拉俊, 沈文宁, 王官充

(西安理工大学 材料学院, 西安 710048)

摘 要: 为了在碳钢表面制备耐磨涂层,使涂层与基体的膨胀系数相近,减少涂层应力,将80% Fe, 13% P, 7% C(质量分数,%)机械混合粉末进行等离子喷涂,制备铁基耐磨涂层。采用粘结剂对偶试样拉伸试验法测定涂层结合强度,采用表面显微硬度法分析涂层硬度,采用MMW-2型(高温)摩擦磨损试验机以40Cr硬质合金为对磨材料对涂层进行耐磨性试验。结果表明,涂层的结合强度平均值为29.16 MPa,显微硬度的平均值为7.889 MPa,高于陶瓷涂层硬度值,涂层的耐磨性能较好,磨损200 min后,涂层的磨损量在36 mg左右,磨损量约为对磨件的1/13,涂层磨损主要为磨粒磨损机制。

关键词: 热喷涂; 硬质涂层; 结合强度; 显微硬度; 耐磨性

中图分类号: TG174 **文献标识码:** A **文章编号:** 0253-360X(2013)04-0027-04



雷阿利

0 序 言

为了增强金属材料表面耐磨性,大多数采用在其表面喷涂陶瓷来提高其表面的硬度和耐磨性^[1-6],但陶瓷材料的熔点、线膨胀系数与金属材料的相差较大,制备的涂层含有较大的残余应力,使涂层在使用过程中易产生裂纹或成片状脱落。为了降低涂层的残余应力,一般采用加过渡层的方法,即利用过渡层材料的线膨胀系数介于基体和涂层之间以降低涂层残余应力,还有采用梯度涂层的方法,即利用涂层材料从与基体结合的底层到面层逐渐过渡的方法来降低残余应力^[7-10],但这些方法对降低涂层残余应力不是很明显,又使制备涂层的工艺变得复杂。如何使制备的涂层残余应力低,涂层制备简单,成为制备耐磨涂层研究的方向。铁基合金粉末与基体的线膨胀系数相近,而喷涂层的硬度高,耐磨性好,可以解决普通陶瓷涂层由于膨胀系数不匹配造成涂层残余应力大的问题。

文中以工业纯铁粉、工业磷铁粉、高纯石墨粉为原料,经机械球磨制成合金粉末,然后用等离子喷涂法制备含非晶态涂层,并且对涂层的结合强度、显微硬度以及耐磨性进行评定,为用等离子喷涂合金粉末制备含非晶涂层提供依据。

1 试验方法

1.1 铁基耐磨涂层的制备

基体材料选用Q235钢,制备涂层时,基体表面先除油,然后进行表面喷砂粗化,喷砂条件及参数为:材料选用刚玉砂,粒度为16~18目,气体为压缩空气,压强为0.6~0.8 MPa,喷砂距离为10~20 mm,喷砂角度保持在60~80°范围内。

喷涂用的铁基粉末是将质量分数为80% Fe, 13% P, 7% C(质量分数,%)三种100目的粉末经球磨机球磨16 h,得到粒径小于50目的混合粉末。将该粉末通过自动送粉连续地输送到GP-80型等离子喷涂设备的喷枪嘴前,在大气环境下,用等离子喷涂法制备硬质涂层。为了确保粉末熔化、雾化良好并且具有一定的加速度,通过查阅文献[11],制定了喷涂工艺参数,电压55 V,电流600 A,氩气压力0.85 MPa,氢气压力0.32 MPa,粉末与喷枪嘴距离4 mm,送粉速度20 g/min,喷涂距离100 mm,喷涂角度60~80°。

1.2 涂层组织结构和性能检测

采用XRD-7000型射线衍射仪测定样品的组织结构。

采用HX-1000型显微硬度计测定各涂层试样的表面硬度,每个试样选五个不同点进行测量,所用载荷为0.5 N,加载时间为15 s,测量5次取平均值,为该试样的硬度值。

采用粘结剂对偶试样拉伸试验法测定涂层结合

强度. 首先对圆柱形试样 A 的端面进行粗化处理, 并进行喷涂, 制成厚度约为 0.3 mm 的涂层. 再将此涂层与同尺寸的经粗化处理的圆柱形试样 B 的端面用高强度粘结剂(高强度粘结剂的质量配比为 E-44 环氧树脂 50 g, 丙酮 4 g, 乙二胺 3 g; 配制方法为将环氧树脂加热至 50~60 °C, 加入丙酮稀释后, 加入乙二胺混合搅拌) 粘结起来, 做成拉伸试样. 将粘结好的对偶试样用夹具夹紧, 注意试样的垂直度, 以免造成偏心. 室温下固化时间 30 min 后, 然后放在 70 °C 烘干箱中进行 30 h 固化处理.

在材料试验机上, 通过测定将涂层从基体上拉开时所用的力及受力面积来计算涂层的结合强度. 为保证静态加载条件, 加载速度应小于 10 mm/min. 试验装置如图 1 所示^[12], 结合强度值可按式(1)进行计算, 即

$$\delta_b = \frac{p}{F_0} \quad (1)$$

式中: σ_b 为涂层结合强度; p 为拉断时的载荷; F_0 为试样截面积.

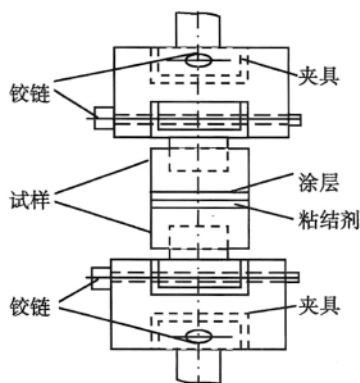


图 1 涂层结合强度测试示意图

Fig. 1 Schematic illustration of coating adhesion

涂层耐磨性能的测定是采用 MMW-2 型(高温)摩擦磨损试验机对涂层进行耐磨性试验, 对磨件为 40Cr 硬质合金. 磨损条件为外加载荷 50 N, 旋转速度 80 r/min, 无任何润滑. 每次磨损 20 min 后, 取下涂层试样, 经清洗烘干后, 在分析天平上称一次质量, 计算其磨损损失重量. 在每次试验前, 用肉眼检查摩擦副和试样表面是否光滑, 是否有划痕和粘着物, 并且做相应的丙酮清洗处理.

2 结果与分析

2.1 涂层的组织性能

对涂层进行 X 射线衍射分析, 结果如图 2 所

示. 由图 2 可见, 在 35° 以及在 40°~50° 之间出现了较为明显的漫射峰, 由此可以证明经等离子热喷涂后涂层中含有部分非晶. 涂层组成主要有 Fe, FeP, Fe₂C, Fe₃C 等相.

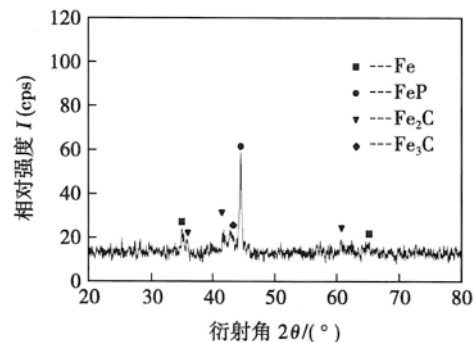


图 2 等离子喷涂法制备的 Fe₈₀P₁₃C₇ 涂层的 XRD 图谱
Fig. 2 XRD profile of amorphous alloy Fe₈₀P₁₃C₇ coating

2.2 涂层结合强度的研究与分析

涂层结合强度在 28.89~29.16 MPa 之间, 结合强度较高. 这主要是由于粉末经过瞬间加热雾化成液态金属颗粒, 飞行速度非常大, 而且在液态金属颗粒撞击基体表面时温度很高(大于 2 000 K), 由于惯性作用, 使液态金属颗粒在基体表面迅速铺展开, 并且与基体之间发生了相互扩散, 即形成了冶金结合. 又由于基体表面经过喷砂预处理, 使表面起伏增加, 最终形成了机械结合与冶金结合相结合的结合方式. 而一般等离子喷涂金属涂层的结合强度为 20 MPa 左右^[13], 因此试验所制备的涂层具有较高的结合强度.

观察涂层试样断裂形式, 基本上都是属于涂层与基材之间的断裂, 而涂层之间的断裂却很少, 说明涂层之间的结合强度高于涂层与基材之间的结合强度.

涂层结合强度的高低与涂层中的残余热应力有关. 在喷涂过程中, 当熔融的粒子高速喷射到温度很低的基材上时, 由于温度梯度的影响, 很容易在涂层内部产生残余热应力, 并且涂层与基材两者的线膨胀系数不同, 所以应力集中现象在涂层与基材结合处尤为明显, 导致涂层与基材间的结合强度小于涂层之间的内聚强度, 因此断裂大多发生在涂层与基材的结合界面处. 随着涂层厚度的增加, 热量也在涂层中逐渐积累, 基材与涂层以及涂层与涂层之间的相对温度差距越来越大, 残余热应力也随之增加, 所以表现为涂层的结合强度逐渐下降. 通过以上的分析可知, Fe₈₀P₁₃C₇ 涂层材料由于粉末主要为铁, 与基体的膨胀系数相近, 又由于喷涂中新相的形成, 消耗了部分能量, 使得涂层的结合强度大于普通

的镍基粉末的结合强度。

2.3 涂层显微硬度的研究与分析

涂层显微硬度的测试结果如图3所示。由图3可见,涂层显微硬度在7.624~8.085 MPa之间,平均值为7.889 MPa。这一硬度值已高于等离子喷涂陶瓷的硬度值^[14],高硬度是由于涂层中含有部分非晶成份,由于非晶相内金属原子的排列是无序的,它不存在晶界、缺陷、偏析等,表现出各向同性,加之铁的熔点较陶瓷低,流动性比陶瓷好,使得涂层较紧密,孔隙和弥散在涂层中的金属间化合物的形成都对涂层硬度的提高起着非常重要的作用。

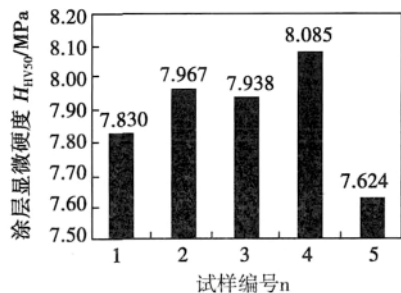


图3 涂层显微硬度测试结果

Fig. 3 Testing result of hardness in coatings

2.4 涂层耐磨损性能的研究与分析

涂层的磨损试验结果如图4所示。磨损200 min后,涂层的磨损量在36 mg左右,而40Cr硬质合金的磨损量在500 mg左右,可见涂层的耐磨性能远远高于40Cr硬质合金。这与涂层的显微硬度高有着密切的关系。图5为涂层磨损后表面微观形貌。由图5可见,经过200 min磨损后,其表面有几条明显的犁沟,还有粘附的小颗粒,这说明磨损是一种磨粒磨损现象,说明非晶态的硬质颗粒被打断后,在磨削面上形成了磨粒,也说明打断的非晶态磨粒硬度较高,从而形成犁沟。

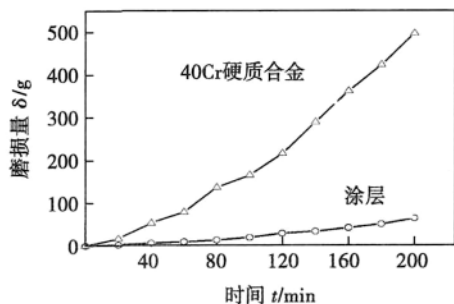


图4 涂层的磨损试验结果

Fig. 4 Wear test curves of plasma sprayed coating

涂层中部分非晶态合金和硬度较高的金属间化

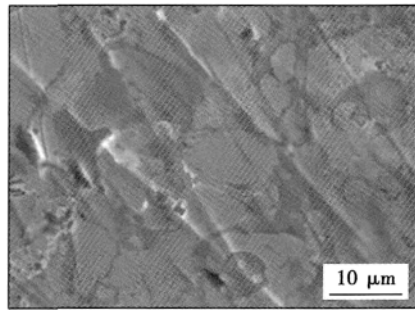


图5 涂层磨损后微观形貌

Fig. 5 Microstructure of amorphous coatings after wear testing

合物存在是涂层耐磨性提高的关键因素。非晶态合金具有较高的硬度和耐磨性的特点,在涂层材料被磨损时,这些非晶态合金成为抗磨的主体。涂层中金属化合物也具有较高硬度,在磨损时,它们共同抵御着外来的对磨材料(40Cr)对涂层的损伤,并能够有效地保护涂层,使涂层表面的磨损量大大地减少。

在磨损初期,涂层中存在的喷涂缺陷如气孔、微裂纹及涂层的致密性对涂层的磨损性能有着一定的影响,尤其是涂层中存在的尺寸比较大的气孔,导致高的应力集中,气孔还可以促使微裂纹的形成,降低涂层以及涂层颗粒之间的结合强度,从而使涂层的磨损性能急剧下降^[15]。

随着摩擦的继续进行,表面空隙下降,涂层的组织致密性提高,硬质相比例增大,使涂层耐磨性提高。综上所述,等离子喷涂法制备的 $\text{Fe}_{80}\text{P}_{13}\text{C}_7$ 合金涂层具有较好的耐磨料磨损性能。

3 结 论

(1) 将球磨后的铁基混合粉末用等离子喷涂方法制备涂层,拉伸试验结果表明,涂层的结合强度平均值为29.16 MPa,高于等离子喷涂金属涂层的结合强度,因此能够满足实际使用需求。

(2) 测试涂层的硬度,其显微硬度(HV_{50})的平均值为7.889 MPa,涂层的硬度值比较高,这一硬度值已高于等离子喷涂陶瓷的硬度值。

(3) 对涂层耐磨性进行研究,磨损摩擦试验表明,涂层的耐磨性能较好,磨损200 min后,涂层的磨损量在36 mg左右,其磨损过程是一个缓慢的逐层磨削过程。

参考文献:

- [1] 陈海涛,李忠盛,孙彩云,等. $\text{Al}_2\text{O}_3/\text{NiCrC}_3\text{C}_2$ 耐磨复合涂

- 层制备及其摩擦学特性研究[J]. 稀有金属材料与工程, 2011, 40(增刊2): 447-451.
- Chen Haitao, Li Zhongsheng, Sun Caiyun, *et al.* Study on $\text{Al}_2\text{O}_3/\text{NiCrCr}_3\text{C}_2$ wearing composite coating and its tribological properties[J]. Rare Metal Materials and Engineering, 2011, 40(S2): 447-451.
- [2] 安家财, 杜三明, 肖宏滨, 等. 等离子喷涂 $40\% \text{ZrO}_2\text{-Al}_2\text{O}_3\text{-}13\% \text{TiO}_2$ 陶瓷涂层及其摩擦磨损性能研究[J]. 表面技术, 2011, 40(2): 4-7.
- An Jiakai, Du Sanming, Xiao Hongbin, *et al.* Study on plasma sprayed $40\% \text{ZrO}_2\text{-Al}_2\text{O}_3\text{-}13\% \text{TiO}_2$ ceramic coatings and tribological properties[J]. Surface Technology, 2011, 40(2): 4-7.
- [3] 李兆峰, 程德彬, 蒋 鹏, 等. 等离子喷涂 $\text{Al}_2\text{O}_3\text{-TiO}_2/\text{MoS}_2$ 陶瓷减摩耐磨涂层的结构与性能研究[J]. 润滑与密封, 2011, 36(11): 93-97.
- Li Zhaofeng, Cheng Debin, Jiang Peng, *et al.* Microstructure and properties of plasma-sprayed $\text{Al}_2\text{O}_3\text{-TiO}_2/\text{MoS}_2$ ceramic coatings[J]. Lubrication Engineering, 2011, 36(11): 93-97.
- [4] 安家财, 杜二明, 肖宏滨, 等. 等离子喷涂 $\text{ZrO}_2/\text{Al}_2\text{O}_3$ 陶瓷涂层的摩擦磨损性能[J]. 中国表面工程, 2011, 24(1): 20-24.
- An Jiakai, Du Erming, Xiao Hongbin, *et al.* Tribological properties of plasma sprayed $\text{ZrO}_2/\text{Al}_2\text{O}_3$ ceramic coatings[J]. China Surface Engineering, 2011, 24(1): 20-24.
- [5] 苗利湘. 等离子喷涂制备铁基复合陶瓷涂层的研究[J]. 金属材料与冶金工程, 2009, 37(5): 7-9.
- Miao Lixiang. Study on fabrication of Fe-based composite ceramic coatings by plasma spraying[J]. Metal Materials and Metallurgy Engineering, 2009, 37(5): 7-9.
- [6] 雷阿利, 李高宏, 冯拉俊, 等. 等离子喷涂 $\text{Cu-Al}_2\text{O}_3$ 梯度涂层的组织与耐磨性分析[J]. 焊接学报, 2008, 29(5): 65-68.
- Lei Ali, Li Gaohong, Feng Lajun, *et al.* Structure and abrasability of $\text{Cu-Al}_2\text{O}_3$ gradient coatings fabricated by plasma spraying[J]. Transactions of the China Welding Institution, 2008, 29(5): 65-68.
- [7] 雷阿利, 杨士川, 冯拉俊, 等. 等离子喷涂 $\text{NiAl}/\text{Al}_2\text{O}_3$ 梯度陶瓷涂层的结构与组织特征[J]. 机械工程材料, 2007, 31(4): 62-65.
- Lei Ali, Yang Shichuan, Feng Lajun, *et al.* Structure of plasma-sprayed $\text{NiAl-Al}_2\text{O}_3$ gradient ceramic coatings[J]. Materials for Mechanical Engineering, 2007, 31(4): 62-65.
- [8] 雷阿利, 李高宏, 冯拉俊, 等. 过渡材料对等离子喷涂 Al_2O_3 梯度陶瓷涂层性能影响[J]. 焊接学报, 2007, 28(10): 25-28.
- Lei Ali, Li Gaohong, Feng Lajun, *et al.* Transition materials for plasma spraying Al_2O_3 gradient ceramic coatings properties[J]. Transactions of the China Welding Institution, 2007, 28(10): 25-28.
- [9] 李高宏, 冯拉俊, 雷阿利, 等. 等离子喷涂 $\text{Cu-Al}_2\text{O}_3$ 梯度涂层与涂层耐磨性分析[J]. 焊接学报, 2008, 29(9): 51-54.
- Li Gaohong, Feng Lajun, Lei Ali, *et al.* Structure and abrasability of $\text{Cu-Al}_2\text{O}_3$ gradient coatings fabricated by plasma spraying[J]. Transactions of the China Welding Institution, 2008, 29(9): 51-54.
- [10] 冯拉俊, 曹凯博, 雷阿利. 等离子喷涂 Al_2O_3 陶瓷涂层的工艺研究[J]. 中国表面工程, 2005, 18(6): 45-48.
- Feng Lajun, Cao Kaibo, Lei Ali, *et al.* Research on the process of plasma sprayed Al_2O_3 ceramic coatings[J]. China Surface Engineering, 2005, 18(6): 45-48.
- [11] 雷阿利, 唐文浩, 冯拉俊. 棒材等离子喷涂法制备 $\text{Fe}_{80}\text{P}_{13}\text{C}_7$ 非晶态合金涂层的成型特征[J]. 焊接学报, 2007, 28(1): 17-18.
- Lei Ali, Tang Wenhao, Feng Lajun. Formation characteristic of $\text{Fe}_{80}\text{P}_{13}\text{C}_7$ amorphous coating fabricated by bar material plasma spray[J]. Transactions of the China Welding Institution, 2007, 28(1): 17-18.
- [12] 徐滨士, 刘世参. 表面工程[M]. 北京: 机械工业出版社, 2001.
- [13] 孙永兴, 王引真, 何艳玲, 等. 离子喷涂工艺稳定性对 Cr_2O_3 涂层结合强度的影响[J]. 兵器材料科学与工程, 2001, 24(2): 38-40.
- Sun Yongxing, Wang Yinzheng, He Yanling, *et al.* Effects of fluctuations of plasma spraying parameters on tension bonding strength of Cr_2O_3 coating[J]. Ordnance Material Science and Engineering, 2001, 24(2): 38-40.
- [14] 周 静, 曹兴进, 张隆平, 等. 等离子喷涂 NiCr 合金基复合梯度润滑涂层的组织与力学性能研究[J]. 表面技术, 2002, 31(3): 17-20.
- Zhou Jing, Cao Xingjin, Zhang Longping, *et al.* Research on microstructure and mechanical properties of plasma sprayed high-temperature self-lubricating composite coating[J]. Surface Technology, 2002, 31(3): 17-20.
- [15] 徐滨士. 纳米表面工程[M]. 北京: 化学工业出版社, 2004.

作者简介: 雷阿利, 女, 1957年生. 教授. 目前主要从事材料的加工与材料的腐蚀与防护方面的教学和科研工作. 发表论文 40 余篇.
Email: leiali@126.com

welding; pulsed laser beam welding; tensile property; cupping property

Effects of keyhole-assisted gas jet on microstructure and microhardness of stainless steel laser weld SHEN Xianfeng , HUANG Wenrong , TENG Wenhua , XU Chao (Institute of Machinery Manufacturing Technology , China Academy of Engineering Physics , Mianyang 621900 , China) . pp 19 – 22

Abstract: Slab CO₂ continuous wave laser welding of HR-2 hydrogen-resistance stainless steel was carried out with different keyhole-assisted gas jet. During welding , the incident angle of the keyhole-assisted gas jet was 60° with a nozzle put ahead of the laser beam. The experimental results show that the layout with gas nozzle ahead of laser beam obtained better weld appearance and had little perturbation on the welding pool than that with gas nozzle behind the laser beam in gas jet-assisted keyhole laser welding. Compared with traditional laser welding , penetration depth increased significantly while penetration width decreased , and the weld shape became gourd-like with narrow middle part and wide upper and lower parts in the enhanced laser welding , because more plasma was suppressed within the keyhole and the keyhole deepened. Shorter columnar grains formed near the fusion line while equiaxed grain existed in the center of weld in enhanced laser welding , and the weld solidified by following ferrite-austenite (FA) mode. The reason for less ferrite precipitated in the weld could be resulted from the introduction of keyhole-assisted gas jet which improved the cooling condition of the weld metal.

Key words: gas jet-assisted keyhole laser welding; assisted gas jet; penetration increase; hydrogen-resistance stainless steel; microstructure

Effect of arc-ultrasonic excitation current on pores and tensile properties of MGH956 alloy TIG weld LEI Yucheng^{1,2} , HUANG Wei¹ , XIA Xiaoping³ , ZHAO Kai¹ , XIAO Bo¹ (1. School of Materials Science and Engineering , Jiangsu University , Zhenjiang 212013 , China; 2. Jiangsu Province Key Laboratory of High-End Structural Materials , Jiangsu University , Zhenjiang 212013 , China; 3. Tianjin Xingang Shipbuilding Heavy Industry Co. , Ltd , Tianjin 300456 , China) . pp 23 – 26

Abstract: The arc-ultrasonic can be excited by modulating the TIG arc through high frequency. The mechanism of arc-ultrasonic was analyzed , and the effect of excitation current on pores and tensile strength of the MGH956 alloy joint made with TIG welding process was investigated. Without arc-ultrasonic , when the excitation current was 5 A and 10 A , pores in the weld obviously grew up , although the amount of pores kept almost the same. When the excitation current increased to 20 A and 30 A , the amount of pores decreased. With arc-ultrasonic , the tensile strength of the resultant joint was improved and reached the optimum value 550 MPa , 76% of that of base metal , when the excitation current was 20 A. The joints fractured with mixed brittle-ductile features.

Key words: MGH956 alloy; arc-ultrasonic; tungsten inert gas welding; pore

Mechanical properties of iron-based hard coatings prepared by plasma spraying technology LEI Ali , FENG Lajun , SHEN Wenning , WANG Guanchong (School of Materials Science and Engineering , Xi'an University of Technology , Xi'an 710048 , China) . pp 27 – 30

Abstract: In order to prepare wear-resistant coating on the surface of carbon steels and make the expansion coefficient of coating close to that of substrate and reduce stress in coating , mechanically mixed powders of 80% Fe , 13% P and 7% C were used to prepare iron-based wear-resistant coating by plasma spraying. The bonding strength was tested using binder dual tensile test method. The hardness in the coating was analyzed by surface microhardness method. And the wear resistance test of coating was carried out by MMW-2 (high temperature) friction and wear testing machine using 40Cr cemented carbide as grinding materials. The results show that the average bonding strength of the coating was 29 MPa , and the average microhardness was 805 HV50 , higher than that of ceramic coating. The coating had better wear resistance , and the coating abrasion loss was around 36 mg which was about 1/13 of the grinding material. And the wear mechanism of the coating was mainly abrasive wear.

Key words: thermal spray; hard coating; bonding strength; microhardness; wear resistance

Effect of material flow on flash formation during continuous driven friction welding JI Shude¹ , LIU Janguang² , ZHANG Liguang¹ , ZOU Aili¹ , FU Li¹ (1. Faculty of Aerospace Engineering , Shenyang Aerospace University , Shenyang 110136 , China; 2. National Key Laboratory for Precision Hot Processing of Metals , Harbin Institute of Technology , Harbin 150001 , China) . pp 31 – 34

Abstract: The 2D coupled thermo-mechanical model was established to numerically simulate the effects of temperature and material flow on the flash formation of ring parts during continuous driven friction welding. The calculated results show that the material in friction stage mainly flew axially , while the radial velocity was nearly zero. During the forging stage , the material in or near the edge of friction surface mainly flew along the radial direction under large axial forging pressure , which resulted in the formation of flash. And the dimensions and bending degree of the flash increased with increasing of welding time , rotating speed and axial forging pressure. Based on the shape of flashes , suitable welding parameters were determined for continuous driven friction welding of 45 steel ring structures.

Key words: continuous driven friction welding; material flow; flash; numerical simulation

Recognition of spatial attitude of welding torch based on swing of rotating arc LI Xiangwen , HONG Bo , YIN Li , HONG Yuxiang (College of Mechanical Engineering , Xiangtan University , Xiangtan 411105 , China) . pp 35 – 37 , 52

Abstract: Based on researches on scanning signal of existing arc sensors , a kind of oscillating rotating arc sensor was put forward. After analyzing the signal characteristics of the new arc sensor , the mathematical relationship between spatial attitude